AGU PUBLICATIONS

JGR

Journal of Geophysical Research: Earth Surface

RESEARCH ARTICLE

10.1002/2013JF002872

Modeling the effects of bed topography on fluvial bedrock erosion by saltating bed load

Shahen A. Huda[1] and Eric E. Small[1]

[1]Department of Geological Sciences, University of Colorado Boulder, Boulder, Colorado, USA

Key Points:
- Existing saltation-abrasion model does not account for topographic irregularity
- Considering bed topography yields orders of magnitude increase in erosion rates
- With bed topography, greatest erosion occurs with small grains and strong flows

Correspondence to:
S. A. Huda,
shahen.huda@colorado.edu

Citation:
Huda, S. A., and E. E. Small (2014), Modeling the effects of bed topography on fluvial bedrock erosion by saltating bed load, *J. Geophys. Res. Earth Surf.*, *119*, 1222–1239, doi:10.1002/2013JF002872.

Received 6 JUN 2013
Accepted 18 FEB 2014
Accepted article online 20 FEB 2014
Published online 11 JUN 2014

Abstract Abrasion by saltation is an important mechanism of fluvial incision into bedrock. Sklar and Dietrich (2004) introduced an abrasion model in which the erosion rate of an "approximately planar" bed is linearly dependent on the kinetic energy transferred by the vertical velocity of saltating grains. However, most bedrock-floored channels exhibit topographic variations that yield deviations from a planar surface, referred to as "bed topography." Observations show that bed topography affects erosion. Here the saltation-abrasion model is extended for a nonplanar bed. A several-centimeter high bump, transverse to the flow, is repeated every 50 cm. The kinetic energy of grain impacts is calculated in two ways: (1) impact velocity normal to bed topography and (2) vertical impact velocity. By comparing the latter case with the planar model, it is possible to isolate the effects of topography on the interception of saltation trajectories. Incorporating bed topography changes erosion in three ways. First, erosion is 10 to 1000 times faster, depending upon transport stage and grain size. Enhanced erosion results from both the interception of grains by topography and the increased kinetic energy transfer associated with high-angle impacts on the stoss side of bumps. Second, erosion increases monotonically with transport stage, whereas maximum erosion occurs at low to intermediate transport stage with a planar bed. Third, erosion decreases monotonically with grain size, whereas maximum erosion occurs with intermediate-sized grains with a planar bed. Although the model is highly simplified, results show that bed topography should be considered when simulating erosion of bedrock.

1. Introduction

Erosion of bedrock-floored channels is a critical process in the evolution of landscapes [e.g., *Howard et al.*, 1994]. However, surprisingly little is known about the physical controls on erosion of bedrock stream beds [*Whipple et al.*, 2000]. Most models of landscape evolution assume that bedrock incision is proportional to flow intensity, combining the effects of rock strength, channel slope, discharge, sediment supply, and sediment characteristics into several parameters not tied to any distinct mechanism [e.g., *Anderson*, 1994; *Tucker and Slingerland*, 1994].

Streams incise into bedrock by several mechanisms, including cavitation [e.g., *Barnes*, 1956; *Allen*, 1971; *Wohl and Ikeda*, 1998], dissolution [e.g., *Allen*, 1971; *Richardson and Carling*, 2005], abrasion by bed load and suspended load [e.g., *Hancock et al.*, 1998; *Whipple et al.*, 2000; *Sklar and Dietrich*, 2001; *Wilson et al.*, 2013], and plucking of rock fragments by fluid shear stresses [e.g., *Allen*, 1971; *Whipple et al.*, 2000]. Since all rivers transport sediment in some quantity, abrasion by bed load is believed to play a fundamental role in fluvial incision into bedrock. To date, models of erosion via sediment abrasion have focused on planar bedrock stream beds [e.g., *Sklar and Dietrich*, 2004]. However, the beds of most bedrock-floored streams exhibit topographic variations that yield deviations from a planar surface, which we refer to as "bed topography." Observations suggest that this bed topography strongly affects erosion [e.g., *Whipple et al.*, 2000]. Here we evaluate the effects of bed topography on modeled erosion of bedrock-floored stream channels.

Particle saltation has been studied in water and air, providing knowledge of the fundamental characteristics of sediment trajectories. This information is necessary to model the erosive effects of saltating sediments. *Einstein* [1950] found saltation length to be a function of particle size, shape, and hydraulic characteristics. Several studies have investigated saltation in water using high-speed photography and videography to determine saltation height, length, and particle velocity [e.g., *Abbott and Francis*, 1977; *Sekine and Kikkawa*, 1992; *Hu and Hui*, 1996a, 1996b; *Chatanantavet et al.*, 2013]. Other studies have simulated saltation trajectories in air [e.g., *Anderson and Haff*, 1988; *Nasrollahi et al.*, 2008] and in water [e.g., *Wiberg and Smith*, 1985;

Lee and Hsu, 1994]. Particles in these simulations are subject to inertia force, submerged weight, lift force, and drag force. In addition to lift due to shear, the Magnus effect creates a lift force due to particle spin [*Rubinow and Keller*, 1961]. These previous studies describe how saltation varies as a function of grain size and transport stage, which are critical components of the bedrock abrasion models described below.

Sklar and Dietrich [2004] presented a physically based model for bedrock incision due to abrasion from saltating bed load using average saltation characteristics taken from several studies. This model states that erosion rate due to saltating bed load is a function of average volume eroded per saltation impact, impact rate, and bedrock exposure. Characteristics of both the impacting grain as well as the bedrock substrate affect the erosive potential of saltating material. Most important to this study, the volume eroded is dependent on the vertical component of particle velocity as it impacts the bed. *Sklar and Dietrich* [2004] predicted maximum erosion at moderate sediment supplies due to tradeoffs between the so-called cover and tools effects and at intermediate transport stage due to tradeoffs between impact energy and frequency.

Erosion occurs due to the transfer of kinetic energy from the impacting particle to the bed, dislodging a volume of rock related to the bed's tensile strength and elasticity. *Sklar and Dietrich* [2004] modeled abrasion of an "approximately planar" river bed. Therefore, they assumed that only kinetic energy associated with the impacting particle's vertical velocity is transferred to the bed causing erosion. However, the majority of erosion due to abrasion is believed to occur where the bed is topographically irregular, with the importance of erosion by suspended sediment increasing for obstructions that protrude higher above the bed [e.g., *Hancock et al.*, 1998; *Whipple et al.*, 2000]. *Sklar and Dietrich* [2004] mentioned that irregular bed topography would increase the fraction of energy that contributes to wear but did not quantify this effect. Here we augment the *Sklar and Dietrich* [2004] model to include bed topography and then evaluate how this fundamental element of bedrock channels affects the relationship between erosion rate, grain size, and transport stage.

Bed topography should affect abrasion by saltating sediment for two reasons. First, saltating grains tend to have vertical velocities on the order of 0.1 m s^{-1} and horizontal velocities on the order of 1 m s^{-1}. Therefore, bed topography can yield impacts that transfer much more kinetic energy to the eroding rock. Second, bed topography may truncate saltation trajectories and therefore increase the impact rate. Bed topography also affects flow characteristics, which could counteract these effects. Increased form drag from bed topography will decrease the boundary shear stress. In addition, a nonplanar bed will increase the threshold for sediment transfer [*Chatanantavet et al.*, 2013]. Together, these effects yield lower transport stage for a nonplanar bed, given the same discharge, slope, and channel geometry.

Johnson and Whipple [2010] addressed the shortcoming of characterizing saltation impacts solely by vertical velocity. Their flume experiments clearly showed that erosion is focused on flow-facing slopes. In light of this, they proposed modification to the *Sklar and Dietrich* [2004] model. Over topography, they speculated that the characteristic velocity transferring energy to the bed may be the horizontal particle velocity rather than the settling velocity. Furthermore, they suggested that with increased roughness, the impact rate will no longer scale with saltation length but with a characteristic roughness length, which will lead to a greater dependence of erosion rates on flow strength. The present study attempts to quantify the energy transferred to the bed by a combination of vertical and horizontal particle velocities.

Chatanantavet and Parker [2009] modified the model presented by *Sklar and Dietrich* [2004] to include a single abrasion capability coefficient, which they claim can be generalized to include nonuniform bed topographies. However, they did not provide any examples to demonstrate the effectiveness of this coefficient. Furthermore, in their adaptation, *Chatanantavet and Parker* [2009] did not explicitly consider impact velocity coefficients.

Planar bedrock stream beds rarely exist in nature. Both *Whipple* [2004] and *Sklar* [2003] noted this limitation of the saltation-abrasion model. Instead, bedrock channel beds are typically sculpted into rounded topography [*Richardson and Carling*, 2005]. Both *Montgomery and Buffington* [1997] and *Merritt* [2001] present classification schemes that define categories of bed morphology, which emphasize that streambeds are usually marked by potholes, flutes, knickpoints, and longitudinal grooves. Erosion is often focused on these features [*Hancock et al.*, 1998; *Whipple et al.*, 2000; *Johnson and Whipple*, 2010; *Wilson et al.*, 2013]. Mechanistic description of incision by abrasion cannot be divorced from the irregular geometry of the riverbed [*Wohl*, 1993; *Wohl and Ikeda*, 1997; *Whipple et al.*, 2000]. Despite this, many studies that investigate

fluvial erosion into bedrock channels do not address the role of bedrock topography in determining erosion rates [e.g., *Howard et al.*, 1994; *Stock and Montgomery*, 1999; *Whipple and Tucker*, 1999, 2002].

Here the model of *Sklar and Dietrich* [2004], including the effects of turbulence [*Lamb et al.*, 2008], is modified for application to a bedrock stream channel with simple bed topography. The goal of this study is not to directly compare the magnitude of erosion for planar and rough beds. This would require a complex numerical representation of the interactions between the flow, bed topography, and sediment, which is beyond the framework established by *Sklar and Dietrich* [2004]. Instead, the intent is to examine how including the effects of bedrock topography changes the modeled relationship between erosion, transport stage, and grain size. For a planar bed, *Sklar and Dietrich* [2004] showed that erosion is maximized at low to moderate flows above a grain size dependent transport threshold. Below, we show that this relationship is fundamentally different when even modest bedrock topography is included. Erosion increases monotonically with transport stage.

A description of how the saltation-abrasion model is modified and applied is presented in section 2. Erosion for a case with bed topography is compared to erosion with a planar bed in section 3. For the case with bed topography, we compare erosion calculated using the normal velocity relative to the local bed surface with erosion calculated using vertical velocity upon impact. The results describe the effects of transport stage and grain size on erosion. In section 4, we discuss the implications of various simplifying assumptions upon which the model results depend. Finally, results from the modified saltation-abrasion model presented here are compared to experimental and field observations from the literature.

2. Model Development

2.1. Existing Model

The model presented here incorporates most of the assumptions made by *Sklar and Dietrich* [2004]. Analysis is limited to abrasion of rock by bed load, neglecting all other mechanisms for stream incision. Rolling and sliding grains are assumed to cause negligible wear; saltating grains are solely responsible for abrasion by bed load. For simplicity, all bed load is assumed to be composed of spherical grains of uniform size.

The model assumes uniform streamflow through the domain. Cross-channel variations in shear stress, local variation in rock strength, and other reach-scale spatial heterogeneities are not accounted for, even though these factors may influence rate of incision by bed load abrasion [*Wobus et al.*, 2006; *Hancock et al.*, 2011].

The *Sklar and Dietrich* [2004] model of erosion by abrasion of a flat bed by saltating sediment grains can be stated as

$$E = V_i I_r F_e, \tag{1}$$

where E is erosion rate, V_i is the volume eroded per impact, I_r is impact rate per unit area, and F_e is the fraction of the streambed that is exposed to streamflow. The elements of the *Sklar and Dietrich* [2004] model are described below and form the basis of the model presented here.

2.1.1. Volume Eroded per Impact (V_i)

Erosion of brittle materials by low-velocity particle impacts occurs through the formation, growth, and intersection of a network of cracks [*Finnie*, 1960]. Though the erosion due to any single impact will depend on the local fracture density, the average wear rate scales with the flux of kinetic energy transferred by the impacting grains [*Engel*, 1976].

The magnitude of the peak tensile stress varies with the component of the impact velocity normal to the bed (v_n) [*Engel*, 1976]. Given the planar-bed approximation, *Sklar and Dietrich* [2004] used the vertical component of impact velocity (w_{si}), where the subscript s refers to the saltating sediment grain and the subscript i indicates impact with the bed. *Sklar and Dietrich* [2004] calculate V_i as

$$V_i = \frac{\pi \rho_s D_s^3 w_{si}^2 Y}{6 k_v \sigma_T^2}, \tag{2}$$

where ρ_s is the sediment density, D_s is the grain diameter, Y is Young's modulus of elasticity, k_v is a dimensionless coefficient, and σ_T is the tensile yield stress of the bed.

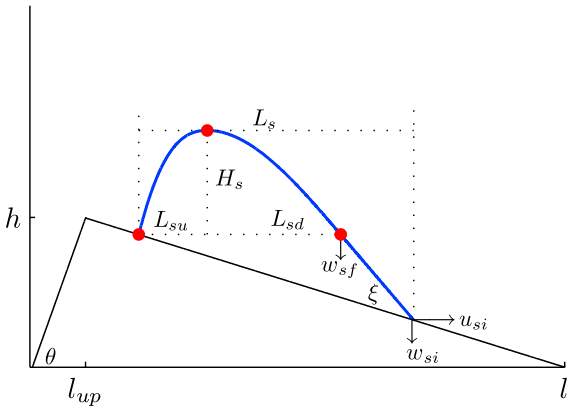

Figure 1. Diagram of saltation trajectory, impact, and topographic parameters. The three red circles show the points a cubic spline is forced through to create the trajectory.

2.1.2. Saltation Characteristics

Sklar and Dietrich [2004] developed empirical expressions for average saltation hop length and height based on analysis of nine experimental and theoretical studies of saltation. These studies used planar beds, so the saltation trajectories were not influenced by bed topography. Instead of accounting for the various forces on individual saltating grains, these regressions of published data constitute a self-consistent description of how saltation trajectories vary as a function of flow strength and grain size. This approach is also used in this study, and so results can be compared with *Sklar and Dietrich* [2004].

Saltation hop height (Figure 1) is calculated as

$$H_s = 1.44 D_s \left(\frac{\tau^*}{\tau_c^*} - 1 \right)^{0.50}, \tag{3}$$

where τ^* is the nondimensional form of the boundary shear stress (τ_b), defined as

$$\tau^* = \frac{\tau_b}{(\rho_s - \rho_w) g D_s}, \tag{4}$$

τ_c^* is the value of τ^* at the threshold of particle motion, ρ_w is the density of water, and g is gravitational acceleration. *Sklar and Dietrich* [2004] used a critical value of nondimensional boundary shear stress of $\tau_c^* = 0.03$. The ratio τ^*/τ_c^* is known as the transport stage and represents flow strength. Regressions are written as functions of nondimensional excess shear stress ($\tau^*/\tau_c^* - 1$) to account for the reduced intensity of particle motion at low excess shear stresses and to force zero sediment transport at $\tau^* = \tau_c^*$. By definition, there is no transport when $\tau^* < \tau_c^*$.

Similarly, average saltation hop length is calculated by

$$\overline{L_s} = 8.0 D_s \left(\frac{\tau^*}{\tau_c^*} - 1 \right)^{0.88}, \tag{5}$$

where the overbar indicates a mean quantity. Later, with the introduction of turbulence, L_s will vary around $\overline{L_s}$. While equations (3) and (5) give information on total saltation hop length and height, the shape of the trajectory is not defined. *Hu and Hui* [1996b] report measurements of total hop length (L_s) and ascending hop length (L_{su}) that indicate a linear relationship, approximated as $L_{su} = \frac{1}{3}\overline{L_s}$. Therefore, the descending portion of the trajectory has average length

$$\overline{L_{sd}} = \frac{2}{3}\overline{L_s}. \tag{6}$$

Sklar and Dietrich [2004] use this $\frac{2}{3}$ factor in estimating the vertical impact velocity (see equation (7) below).

2.1.3. Vertical Impact Velocity (w_{si})

None of the studies analyzed by *Sklar and Dietrich* [2004] include direct measurements of the vertical component of impact velocity (w_{si}). However, *Sklar and Dietrich* [2004] argued that the mean sediment particle descent velocity (w_{sd}) can be written as

$$w_{sd} = 0.4 (R_b g D_s)^{1/2} \left(\frac{\tau^*}{\tau_c^*} - 1 \right)^{0.18}, \tag{7}$$

where $R_b = \rho_s/\rho_w - 1$ is the nondimensional buoyant density of sediment. Using data from *Abbott and Francis* [1977] and *Wiberg and Smith* [1985], *Sklar and Dietrich* [2004] estimated that on average, the vertical velocity when the particle reaches the same elevation as takeoff ($\overline{w_{sf}}$) is

$$\overline{w_{sf}} \approx 2 w_{sd}. \tag{8}$$

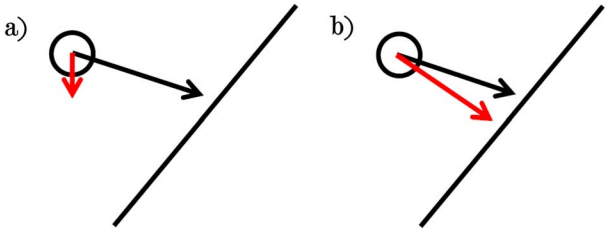

Figure 2. Schematic of (a) w_{si} versus (b) v_n, where the black arrow is the velocity of the particle impinging on the surface (black line) on a trajectory like 3 from Figure 3 and the red arrow represents w_{si} and v_n, respectively.

As with $\overline{L_s}$, the overbar indicates a mean quantity around which w_{sf} will vary with the introduction of turbulence. *Sklar and Dietrich* [2004] use $\overline{w_{sf}}$ as an estimate of w_{si} for their case of planar topography. Here determining w_{sf} is one step in estimating v_n.

2.1.4. Exposed Fraction (F_e)

The exposed fraction of the bed defines the proportion of saltation impacts that can actually remove volume. *Sklar and Dietrich* [2004] defined F_e as

$$F_e = 1 - \frac{q_s}{q_t} \tag{9}$$

for $q_t \geq q_s$, and $F_e = 0$ if $q_s > q_t$, where q_s is the sediment mass flux per width and q_t is the stream's sediment transport capacity per width. *Sklar and Dietrich* [2004] used the *Fernandez-Luque and van Beek* [1976] bed load sediment transport relation to define q_t,

$$q_t = 5.7\rho_s(R_b g D_s^3)^{1/2}(\tau^* - \tau_c^*)^{3/2}\,. \tag{10}$$

While a linear description of the cover effect is simple and straightforward, other formulations of F_e have been proposed. For example, *Turowski et al.* [2007] presented an exponential model from a probabilistic argument. This model of F_e has been implemented with success [e.g., *Turowski et al.*, 2008]. More realistically, *Hancock and Anderson* [2002] suggested that the thickness of the alluvial cover is important in determining the exposed fraction. This approach allows changes in sediment load through the river's history to affect the extent of alluvial cover in the future and reflects the reality of the situation much better than a ratio of sediment flux to transport capacity. However, for consistency with *Sklar and Dietrich* [2004], equation (9) is used here.

2.1.5. Impact Rate (I_r)

The rate of saltation impacts on the bed, per unit area and per unit time (I_r), is proportional to the flux of bed load particles and inversely proportional to the downstream distance between impacts. Therefore, *Sklar and Dietrich* [2004] wrote the impact rate as

$$I_r = \frac{6q_s}{\pi\rho_s D_s^3 \overline{L_s}}\,. \tag{11}$$

Importantly, the impact rate decreases with increasing $\overline{L_s}$ and therefore increasing transport stage.

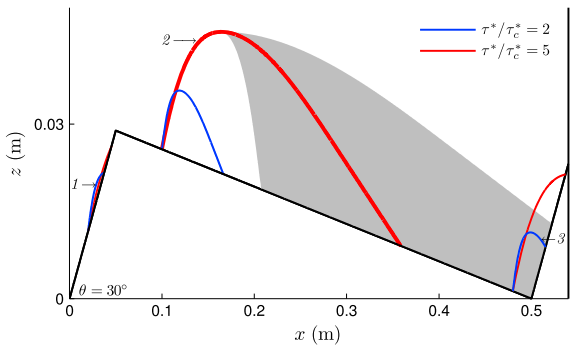

Figure 3. Sample trajectories for $D_s = 7$ mm at two different flow strengths from three takeoff locations over topography defined by $\theta = 30°$, $l_{up} = 0.05$ m and $l = 0.5$ m (vertical exaggeration ≈ 6.5). Given turbulence, trajectory 2 could fall anywhere within shaded region (see section 2.2.5). Examples of the three types of impacts are shown: (1) upslope ascending; (2) downslope; and (3) upslope descending.

2.2. Modifications to the Model

When introducing bed topography, it becomes necessary to explicitly define the saltation trajectory to determine sediment impact locations and impact characteristics. With nonplanar topography, the angle at which the grain impacts the topography becomes relevant (ξ), and the normal impact velocity (v_n) must replace the vertical impact velocity (w_{si}) in equation (2). Since this velocity is squared, the difference between w_{si} and v_n is significant in determining V_i on nonplanar surfaces (see Figure 2). Similarly, the downstream distance traveled during a single hop can be greater than or less than $\overline{L_s}$, as shown by the various trajectories in Figure 3. The hop trajectory and v_n are defined more completely in section 2.2.2.

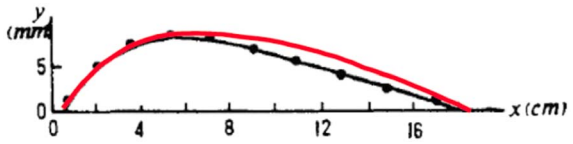

Figure 4. Measured trajectory (black line) from *Hu and Hui* [1996a] and modeled trajectory (red line) based on H_s, L_s, and L_{su} and using cubic splines.

2.2.1. Topography

The *Sklar and Dietrich* [2004] model applies strictly to sections of streams with planar beds. The modified model presented here is applied to simple repeating bed topography that is oriented transverse to the flow direction (see Figure 3). A topographic rise is defined by the angle of its stoss slope (θ), its total length (l), and the horizontal length of the stoss slope (l_{up}). The analysis presented here relies on the base case with $l = 50$ cm, $l_{up} = 5$ cm, and $\theta = 30°$, yielding a bump height of 2.9 cm. The sensitivity to these parameters is analyzed in section 3.3. The topography is repeating, such that a saltating grain will continually encounter identical terrain as it moves downstream. The scale of the topography is much larger than the sediment grains ($D_s = 1 - 20$ mm), allowing saltating grains to be treated as point particles. Finally, the mean slope of the channel is not considered in the calculations because it is negligible compared to the slopes of the stoss and lee sides of the bump.

2.2.2. Trajectory

It is assumed that topography does not impact the flow enough to change basic saltation hop characteristics (e.g., $\overline{L_s}$, H_s, and $\overline{w_{sf}}$). The impact of this assumption on the results is discussed in section 4. Saltation trajectories are simulated using cubic splines [*D'Errico*, 2009]. Trajectories are forced to go through the takeoff point, a point L_{su} downstream of takeoff and H_s above takeoff, and a point $\overline{L_s}$ downstream of takeoff and at the takeoff elevation (Figure 1). Furthermore, trajectories are forced to be concave down and have negative curvature. Modeled trajectories using these parameters fit very well with published trajectories [*Hu and Hui*, 1996a], as shown in Figure 4. The takeoff angle (ψ) is not specified but instead calculated based on the cubic spline fit to trajectory. It is calculated by $\left.\frac{\partial z}{\partial x}\right|_{x=0}$, where z and x are the vertical and horizontal positions of the saltating grain, respectively. In some cases, $\psi < \theta$ and the particle rolls up the face, causing no erosion.

2.2.3. Combining Saltation and Topography

In the most basic sense, each simulated saltation hop takes off from one point on the given topography and lands at another, eroding a small volume from the surface according to equation (2). However, determining the impact location is not as simple as adding $\overline{L_s}$ to the takeoff location, due to changes in elevation between takeoff and impact. Therefore, the impact characteristics cannot be determined by the model presented by *Sklar and Dietrich* [2004].

Because the topography is large compared to the saltation trajectories, impacts can occur on both the ascending and descending portions of the trajectory (Figure 3). The differences in impact characteristics this creates are discussed next.

2.2.4. Impact Characteristics

Saltating grains can impact the bed topography while they are either descending or ascending. While the physics of these impact scenarios are identical, the components of impact velocity must be determined differently depending on whether the impact occurs on the particle's ascent or descent.

2.2.4.1. Descending Case

Particles impact the bed during the descending limb of their trajectories on both the stoss and lee sides of the bump, depending on their takeoff position (Figure 3). It has been shown that horizontal velocity of a saltating grain along its descent is nearly constant [*Hu and Hui*, 1996a]. For example, in the trajectory shown in Figure 4, the horizontal velocity of the particle changes by less than 5% along the descent. This constant velocity can be determined by geometry, as

$$\frac{\overline{w_{sf}}}{u_{sd}} = -\left.\frac{\partial z}{\partial x}\right|_{x=\overline{L_s}}, \tag{12}$$

where u_{sd} is the horizontal velocity of the saltating particle along its descent.

The horizontal impact velocity (u_{si}) is taken to be equal to u_{sd} along the descent. Extending equation (12) to the case of impact, the vertical impact velocity (w_{si}) is taken as

$$w_{si} = -u_{si}\left.\frac{\partial z}{\partial x}\right|_i. \tag{13}$$

The spatial derivative ($\partial z/\partial x$) is known at all x, allowing for simple evaluation of equations (12) and (13). The negative signs in equations (12) and (13) reflect that a positive vertical particle velocity (w_s) is in the $-z$ direction. Since $z(x)$ has negative curvature, equation (13) implies that hops shortened by topography will impact with slower vertical velocities than predicted by *Sklar and Dietrich* [2004], hops that impact at the same elevation as takeoff will have vertical velocities equal to those predicted by *Sklar and Dietrich* [2004], and hops that are lengthened due to topography will impact faster in the vertical than predicted by *Sklar and Dietrich* [2004]. These vertical impact velocities will not be much greater than those predicted by *Sklar and Dietrich* [2004] since $\partial z/\partial x$ does not change much when z is below takeoff elevation.

2.2.4.2. Ascending Case

For the case in which a saltating grain impacts the bed while it is still rising along its trajectory, like trajectory 1 in Figure 3, a different set of equations is needed to determine the impact characteristics. *Sklar and Dietrich's* [2004] data analysis show that the average horizontal particle velocity over the duration of a hop that takes off and lands at the same elevation is

$$\overline{u_s} = 1.56(R_b g D_s)^{1/2}\left(\frac{\tau^*}{\tau_c^*} - 1\right)^{0.56}. \tag{14}$$

For this condition to be true while equation (13) is also true, then along the ascent,

$$u_{su} = 3\overline{u_s} - 2u_{sf}, \tag{15}$$

where u_{su} is the horizontal velocity of the particle along its ascent. As in the descending case, $u_{si} = u_{su}$ along the ascent. The vertical impact velocity is solved for using equation (13).

2.2.4.3. Normal Impact Velocity (v_n)

While expressions for w_{si} and u_{si} are relatively easy to obtain, equation (2) requires an estimate of v_n. The component of impact velocity normal to the surface requires knowledge about the impact speed (S_i) and impact angle (ξ). Since w_{si} and u_{si} are orthogonal, S_i is

$$S_i = \sqrt{w_{si}^2 + u_{si}^2}. \tag{16}$$

If the impact angle (ξ) is considered as the angle between the bedrock surface and the particle trajectory, then v_n is

$$v_n = S_i \sin\xi. \tag{17}$$

2.2.5. Effects of Turbulence

Simulating individual saltation hops using the previously defined equations requires identical hop trajectories for grains of equal size. Obviously, this is not the case in nature. The randomness of turbulence in streamflow drives this variability. *Lamb et al.* [2008] expanded on the *Sklar and Dietrich* [2004] model to include turbulence. In this approach, a normal distribution is applied to w_{sf} to account for vertical fluctuations in the flow field. These fluctuations have standard deviation approximately equal to the friction velocity (u_*) [*Nezu and Nakagawa*, 1993]. Therefore, each hop has w_{sf} defined by

$$w_{sf} = \overline{w_{sf}} + w', \tag{18}$$

where $\overline{w_{sf}}$ is defined by equation (8), and w' is a random number from a truncated normal distribution with mean zero and standard deviation u_*, such that $-\overline{w_{sf}} < w' \leq 6u_*$ [*Lamb et al.*, 2008]. The friction velocity is defined by $u_* = (\tau_b/\rho_w)^{1/2}$.

This variability in w_{sf} forces variability in L_{sd}; an increase in w_{sf} means that the saltating grain will fall from H_s faster. This more rapid fall necessarily decreases L_{sd}. Descending hop length deviates from $\overline{L_{sd}}$ as

$$L_{sd} = \frac{\overline{w_{sf}}}{w_{sf}}\overline{L_{sd}}. \tag{19}$$

Other saltation characteristics (e.g., u_{si}, S_i, and v_n) are defined by equations (12), (16), and (17) using the deviatoric quantities w_{sf} and L_{sd} from equations (18) and (19). Saltation characteristic quantities H_s and L_{su} are unaffected by w'.

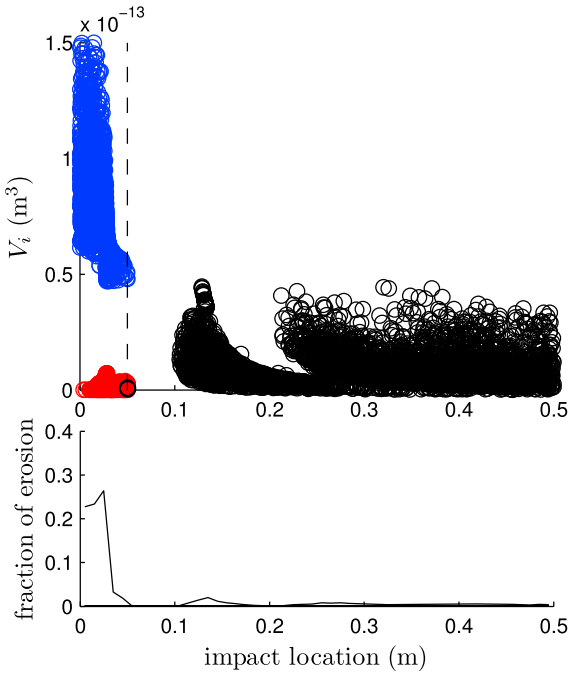

Figure 5. (top) Spatial distribution of V_i for a bump-normal model run with $D_s = 5$ mm, $\tau^* / \tau_c^* = 4$, $\theta = 30°$, $l = 0.5$ m, and $l_{up} / l = 0.1$. The vertical dashed line shows the x position of the crest of the bump: stoss side to the left, lee to the right. Blue points are upslope-descending impacts, red points are upslope-ascending impacts, and black points are downslope impacts. (bottom) The fraction of total erosion as a function of location in 1 cm increments.

2.2.6. Impact Rate (I_r)

With topography, the actual length of each saltation hop is not $\overline{L_s}$. Therefore, it does not make sense to calculate impact rate according to equation (11). Instead, the impact rate per unit area is calculated through the simulation of n successive hops, representing a population of particles traversing the topography with takeoff points spanning the domain. While ascending, the grain is assumed to travel with horizontal velocity u_{su} (defined by equation (15)). On the descent, the particle is assumed to travel at u_{sf} (defined by equation (12)). With these assumptions, the total time (t_{tot}) and distance traveled (s_{tot}) are calculated. These quantities can be broken into time spent and distance traveled above the upslope (t_u, s_u) and downslope (t_d, s_d). The simulation is further assumed to have unit width ($W = 1$). With this assumption, distances can be transformed to areas traversed (A_{tot}, A_u, A_d).

Impact rates are calculated on the upslope as

$$i_u = \frac{n_u}{t_u A_u}, \tag{20}$$

where n_u is the number of impacts on the upslope. A similar quantity i_d is calculated using corresponding quantities for the downslope. To extend i_u and i_d to impact rates for a section of stream with a known sediment flux per width q_s, the mass flux per particle per width (m) is calculated as

$$m = \frac{\pi \rho_s D_s^3}{6 t_{tot} W}. \tag{21}$$

Therefore, the particle flux per width is q_s/m, and total impact rates per width for the upslope can be calculated as

$$I_{r,u} = i_u \frac{q_s}{m}. \tag{22}$$

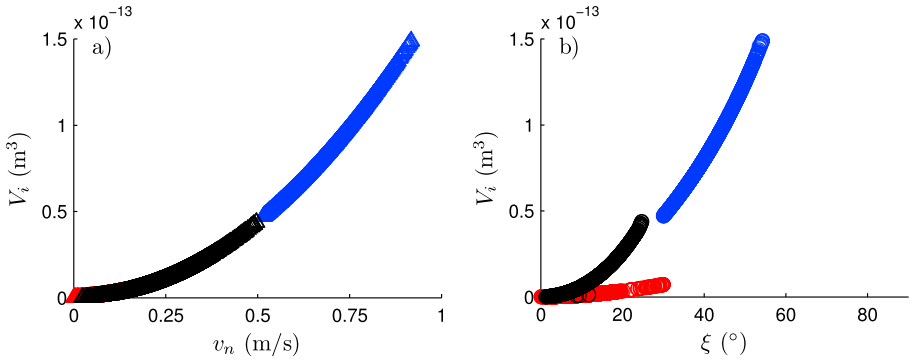

Figure 6. V_i as a function of (a) v_n and (b) ξ for a bump-normal model run with $D_s = 5$ mm, $\tau^*/\tau_c^* = 4$, $\theta = 30°$, $l = 0.5$ m, and $l_{up}/l = 0.1$. Blue points are upslope-descending impacts, red points are upslope-ascending impacts, and black points are downslope impacts.

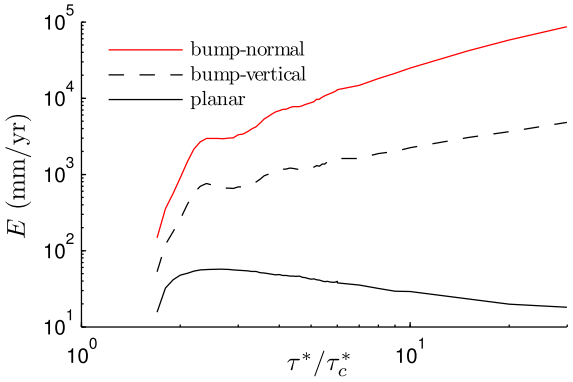

Figure 7. Erosion (E) versus transport stage (τ^*/τ_c^*) for the planar, bump-normal, and bump-vertical models, using $D_s = 60$ mm, $l = 0.5$ m, $l_{up}/l = 0.1$, $\theta = 30°$, and $q_s = 2.37$ kg m^{-1} s^{-1}.

An impact rate for the downslope ($l_{r,d}$) is similarly calculated. These impact rates are used in equation (1) to determine erosion rates along the upslope and downslope (E_u, E_d). An estimate of the net erosion rate along the entire domain (E) is made using a weighted average of E_u and E_d. That is,

$$E = \frac{l_{up}}{l} E_u + \left(1 - \frac{l_{up}}{l}\right) E_d, \qquad (23)$$

where l_{up} is the horizontal distance covered by the upslope ($l_{up} = h \cot \theta$).

2.3. Model Algorithm and Experiments

The model simulates a single saltating grain traversing the topography many times given a wraparound boundary condition. The number of simulated hops (n) is specified, as are the quantities related to sediment and bed characterization, topography, and flow strength. The particle is assigned a random initial location. For each hop, H_s is assigned by equation (3), and L_s is assigned by equations (5) and (19). A trajectory is fitted to the assigned points, and the intersection between topography and the fitted trajectory is found. From this point, impact characteristics are determined and an eroded volume (V_i) is calculated. Throughout the trajectory, the particle's horizontal velocity and position are tracked to create measurements of time traversing both the upslope and downslope (t_u, t_d), allowing for calculation of l_r.

We show below that erosion is focused on the stoss side of topographic bumps. However, we do not allow the topography to evolve as a result of this nonuniform erosion. Accounting for the feedbacks between bed topography, impact location, and the distribution of erosion is beyond the scope of the current effort. The maintenance and creation of bed topography is at least partly controlled by rock structure and plucking, which is not represented by the modeling framework used here. So, an abrasion-only model is not appropriate to simulate the evolution of bed topography.

The results shown below are based on three variants of the saltation-abrasion model. First is the original *Sklar and Dietrich* [2004] model: topography is planar and erosion is based on kinetic energy associated with vertical velocity at grain impact. We refer to this model as "planar." Second is the variant described in section 2.2: a topographic bump erodes according to kinetic energy transfer associated with normal velocity at grain impact (referred to as "bump-normal"). The prescribed bed topography would affect boundary shear stress and the threshold for sediment transfer. Increased form drag from the nonplanar bed will decrease τ^* compared to the planar case. Simultaneously, a nonplanar bed will increase τ_c^* [e.g., *Chatanantavet et al.*, 2013, Table 2]. Thus, transport stage will be lower for the nonplanar case, given the same discharge, slope, and channel geometry. Calculating changes in τ^*/τ_c^* due to bed topography is beyond the scope of this effort. Therefore, we focus our comparison of these two models on how erosion varies with transport stage (i.e., with equal τ^*/τ_c^*). In the discussion, we comment on how the simulated erosion values would compare at equal discharge.

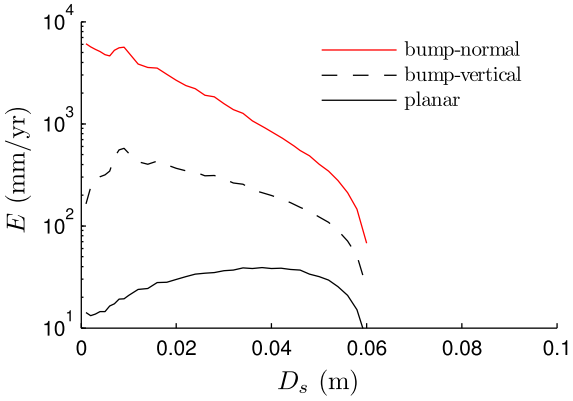

Figure 8. Erosion (E) versus grain size (D_s) for the planar, bump-normal, and bump-vertical models, using $\tau_b = 48.6$ Pa, l = 0.5 m, l_{up}/l = 0.1, $\theta = 30°$, and $q_s = 2.37$ kg m^{-1}s^{-1}. Note that transport stage decreases with grain size because τ_b is held constant.

We use a third variant of the model to more fully understand our results: a topographic bump is identical to the nonplanar case, but erosion is based on vertical impact velocity only ("bump-vertical"). By comparing the two cases with bumps, we quantify the effects of using the normal velocity in

Table 1. Model Output Summary for Case With $l = 0.5$ m, $l_{up}/l = 0.1$, $\theta = 30°$, $D_s = 5$ mm, and $\tau^*/\tau_c^* = 4$[a]

Model	Category	V_i ($\times 10^{-14}$ m^3) 5%–95%	v_n or w_{si} (m/s) 5%–95%	ξ (deg) 5%–95%	% Impacts	% Erosion
Bump-normal	downslope	0.15–2.53	0.093–0.378	5.2–19.7	49.6	22.7
	upslope ascend	0.03–0.30	0.042–0.129	5.4–18.4	29.6	2.3
	upslope descend	5.28–12.37	0.546–0.836	32.0–49.8	20.8	75.0
Bump-vertical	downslope	0.45–3.51	0.159–0.445	5.2–19.7	49.6	82.9
	upslope ascend	0–0	0–0	5.4–18.4	29.6	2.3
	upslope descend	0.02–2.43	0.036–0.370	32.0–49.8	20.8	17.1
Planar		0.24–3.43	0.118–0.440			

[a]Category indicates the location and type of impact, as shown in Figure 3. Data in the fourth column are v_n for the bump-normal model and w_{si} for the bump-vertical and planar models.

calculations of erosion. Bed topography is identical for these two variants, so this comparison is made at equal discharge and equal transport stage. By comparing the third variant (bump-vertical) with the original planar *Sklar and Dietrich* [2004] model, we isolate the effects of topography on the impact rate of saltating grains.

3. Results

We first analyze an example model run to describe the distribution of n impacts over the topography, as well as produce single values of E, E_u, and E_d over the domain. Both types of output are instructive, informing where erosion is focused as well as the rate of erosion.

3.1. Eroded Volume per Impact

First we describe the basic behavior of the bump-normal model. For this model, the grain-bed impacts fall into three categories (see Table 1). First, there are impacts on the downslope that all occur on the particle's descent. These impacts are fairly low angle and have a small normal velocity. For the base case, where $D_s = 5$ mm, $\tau^*/\tau_c^* = 4$, $\theta = 30°$, $l = 0.50$ m, and $l_{up}/l = 0.1$, these impacts are characterized by $\xi < 25°$ and $v_n < 0.40$ m s^{-1}. Second, there are impacts on the upslope along the particle's ascent. These impacts are also low angle ($< 25°$) with low normal velocity (< 0.2 m s^{-1}). In the third category, where impacts occur on the descent along the upslope, eroded volume per impact is greater than the other categories due to greater normal velocities and impact angles (for the base case, $\xi > 30°$ and $v_n > 0.5$ m s^{-1}). Schematics of these trajectories can be seen in Figure 3. While this third category has proportionately fewer impacts, these impacts dominate the erosion: 21% of the impacts account for 75% of the total eroded volume.

Characteristics of impacts for the bump-vertical and planar model are also presented in Table 1. In the bump-vertical model, the ascending impacts do not erode volume. Only half the impacts in the bump-vertical occur on the downslope (identical to bump-normal), but these impacts yield more than 80% of the erosion. In the bump-vertical model, these impacts are relatively more efficient than upslope-descending impacts because they impact the bed with greater vertical velocity: the 5%–95% interval of w_{si} of downslope impacts is 0.159–0.445 m/s but only 0.036–0.370 m/s for upslope-descending impacts. This is very different behavior from the bump-normal case, where upslope-descending impacts are the most efficient.

Table 2. Model Parameter Input Values Corresponding to the South Fork Eel River, California

Input	Symbol	Value
Sediment supply	q_s	2.37 kg/m s
Rock tensile strength	σ_T	7.0 MPa
Rock elastic modulus	Y	5.0×10^4 MPa
Dimensionless rock resistance parameter	k_v	1.0×10^6
Sediment density	ρ_s	2650 kg/m^3
Water density	ρ_w	1000 kg/m^3

For the bump-normal model, the spatial distribution of volume removed, V_i, shows that the impacts that remove the most volume ($V_i > 0.5 \times 10^{-13}$ m^3) are located on the upslope (Figure 5). These impacts represent the third category (upslope descend). As shown in Table 1, V_i for these impacts is an order of

Table 3. Fraction of Impact Types for Three Different Grain Sizes, Using the Bump-Normal Model

Impact Type	$D_s = 1$ mm	$D_s = 20$ mm	$D_s = 60$ mm
Downslope	0.22	0.54	0.77
Upslope ascend	0.10	0.01	0.00
Upslope descent	0.68	0.45	0.23

magnitude greater than for any other type of impact, across all three variations of the model. The upslope impacts associated with relatively low eroded volume ($V_i < 0.1 \times 10^{-13}$ m^3) represent the second category (upslope ascend). In Figure 5, the area with no impacts (between 0.05 and approximately 0.10 m) represents a shadow zone, where particles taking off on the upslope cannot land due to the geometry of their trajectories. The lens of no impacts within the swath of downslope impacts represents the difference between the two major types of downslope impacts. Impacts to the left of the lens represent particles that have hopped up over the crest of the bump, whereas impacts downstream of the lens represent particles that have taken off from the downslope and landed farther downstream.

Saltating particles that erode large volumes impact the bed with high normal velocities, as V_i scales with the square of v_n (see equation (2)). High normal velocity can be due to either a high speed at impact or an impact angle approaching perpendicularity (see equation (17)). The interplay between V_i, v_n, and ξ is shown in Figure 6. The three impact types are again clear, with impacts associated with high eroded volume occurring along the upslope at high angles and normal velocities.

3.2. Erosion Rates

Combining the V_i record with calculated impact rates (I_r) and the exposed fraction of the bed (F_e) allows calculation of an erosion rate (E) that determines how quickly the bed is lowered (equation (1)). The model requires certain parameters to characterize bedrock properties as well as the sediment flux downstream. Here values used are meant to approximate a gauged reach of the South Fork Eel River, California, and are taken from *Sklar and Dietrich* [2004] (see Table 2). Even though the erosion rates presented below have units of "mm/yr," they are not intended to represent realistic long-term values. Instead, they represent the erosion rate at a particular transport stage, scaled to an annual rate. The actual rate of channel lowering would be much lower, given that transport events are infrequent.

We first compare how E varies with transport stage across the three variants of the model. For a planar bed, E is greatest at relatively low flows, just above the sediment transport threshold (Figure 7). For stronger flows, E decreases monotonically as τ^*/τ_c^* increases. This is one of the basic results described by *Sklar and Dietrich* [2004], which they attributed to greater hop length and decreasing impact rate as transport stage increases. In Figure 7, τ^*/τ_c^* values were chosen to match the corresponding plots from *Sklar and Dietrich* [2004].

The introduction of bed topography yields two important changes. First, the erosion rates calculated for cases with topography are much higher than that for the planar bed. Erosion is roughly 10 times higher at low transport stage and more than 100 times higher at high transport stage. Second, there is a fundamental change in model behavior once topography is introduced: erosion rate increases monotonically with transport stage (Figure 7). The behavior of the two nonplanar models is very similar. This indicates that the interception of saltating grains by bed topography is responsible for E increasing with transport stage. Calculating erosion based on normal velocity at impact simply increases the magnitude of erosion but does not change the relationship between E and transport stage. This is expected given that normal velocity is much greater than vertical velocity, particularly on the stoss side of the bump where impact angle is roughly 40° (Table 1).

We next compare how E varies with grain size for the three models. Values were again selected to match the corresponding plots in *Sklar and Dietrich* [2004]. The sediment supply is constant in Figure 8, but transport stage decreases with grain size. The variations in erosion with grain size reflect the interplay between volume eroded per impact, the impact rate, and the fraction of bed exposed. For the planar bed, maximum erosion occurs at intermediate grain sizes [*Sklar and Dietrich*, 2004]. For smaller grain sizes, erosion is lower because vertical impact velocity, and thus V_i, is very low.

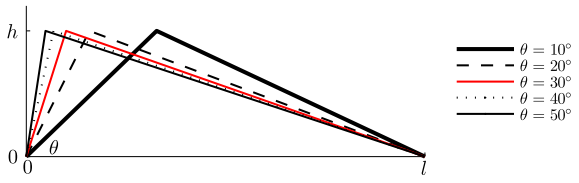

Figure 9. Topography with varying θ. Height is kept constant at 0.029 m, and the total length is kept constant at $l = 0.50$ m.

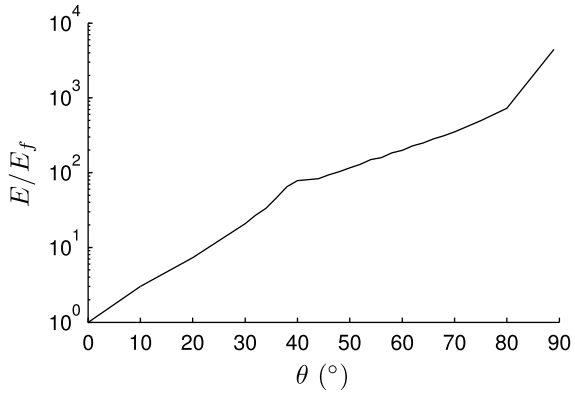

Figure 10. Ratio of erosion in the bump-normal and planar models (E/E_f), using $D_s = 4$ mm, $\tau^*/\tau_c^* = 5$, and $q_s = 0.237$ kg m^{-1} s^{-1}. For all nonzero θ, the bump height is equal to 0.029 m. For all cases, $l = 0.5$ m.

For larger grains, V_i is much greater. However, F_e decreases strongly with grain size, so no kinetic energy is transferred to the bedrock if D_s is too great.

First, we describe results from the bump-normal case. Again, the introduction of bed topography yields an important change in model behavior: erosion rate decreases monotonically with grain size (Figure 8) given a constant basal shear stress (τ_b). This is consistent with the previous result (Figure 7), given that transport stage is greatest for small grain sizes. The difference in erosion between the bump-normal case and the planar case is greatest at small grain sizes. In the bump-normal case, small grains yield significant V_i. A majority of the impacts for small grains are on the upslope during descent at high-impact angle (Table 3). Therefore, the kinetic energy transfer depends strongly on the horizontal velocity of small grains, which is not negligible as is the case for their vertical velocity. The bump-vertical case yields an intermediate result. Erosion decreases with grain size, except for the smallest grains. Because V_i is based on vertical velocity in this case, the smallest grains yield little erosion. This is only partially offset by increases in the impact rate resulting from interception of grains by the bed topography. In Figure 8, there is a hump at $D_s \approx 0.01$ m in both nonplanar cases. This is discussed in the next section.

3.3. Sensitivity Analysis

The above analysis relies on a specific geometry to determine the effects of bed topography. To evaluate how the geometry of the topography affects the results, the sensitivity of the model to changes in the angle of the stoss side of the bump, θ, is tested. To illustrate the effect of θ on erosion enhancement (E/E_f), the model was run at a fixed grain size and flow strength for θ values between 0° and 90°, keeping the height of the bump equal for all runs (see Figure 9). Only the bump-normal and planar models were used for the sensitivity analysis. These results are presented in Figure 10.

Erosion enhancement increases monotonically with θ. The steeper the slope, the greater the erosion enhancement due to topography. As the slope becomes steeper, u_{si} plays a larger role in determining v_n. Since u_{si} is roughly 15 times greater than w_{si} in the base case, maximizing the energy transferred to the bed by downstream motion of saltating grains will maximize erosion rates.

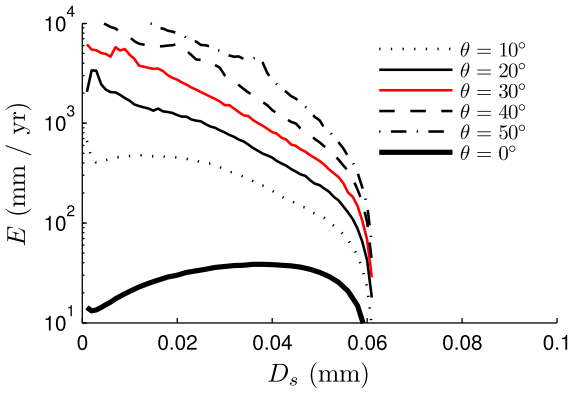

Figure 11. Effect of θ on bump-normal E with varying D_s for a flow with $\tau_b = 48.6$ Pa and $q_s = 2.37$ kg m^{-1} s^{-1}. The $\theta = 30°$ line is the same as the bump-normal line in Figure 8. The $\theta = 0°$ line is the same as the planar line in Figure 8. For all nonzero θ, bump height is equal to 0.029 m. For all θ, $l = 0.5$ m.

This trend of increasing E with increasing θ is consistent across a range of grain sizes and flow strengths. Regardless of θ, the trends of E decreasing with D_s and increasing with τ^*/τ_c^* are apparent (Figures 11 and 12). Thus, the important differences between the results from this study and from *Sklar and Dietrich* [2004] in how E varies with D_s and transport stage are consistent with all θ. It is also clear from Figures 11 and 12 that any bed topography, no matter how gentle, greatly increases erosion rate. This shows that whenever the downstream particle velocity (u_{si}) transfers energy to the bed and topography exists to intercept saltation trajectories, erosion rates are greatly enhanced.

The curves in Figures 11 and 12 are not smooth. This is similar to the bump

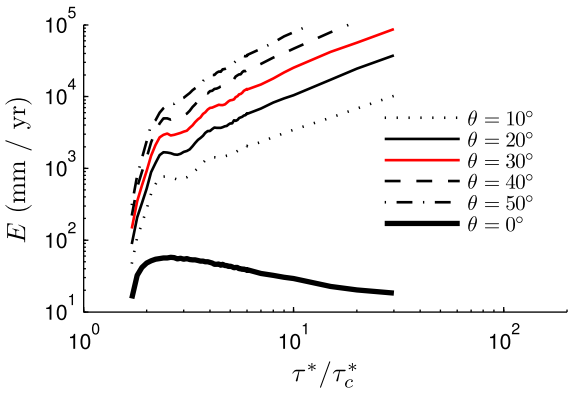

Figure 12. Effect of θ on bump-normal E with varying τ^*/τ_c^* with $D_s = 60$ mm grains and $q_s = 2.37$ kg m^{-1} s^{-1}. The $\theta = 30°$ line is the same as the bump-normal line in Figure 7. The $\theta = 0°$ line is the same as the planar line in Figure 7. For all nonzero θ, the bump height is equal to 0.029 m. For all θ, $l = 0.5$ m.

observed in Figures 7 and 8. The position of the irregularities varies with D_s in Figure 11. The irregularities are related to interactions between the hop height and length and the height and length of the stoss face, as shown by the nonuniform spatial distribution of V_i in Figure 5. Local peaks in erosion exist where the combination of flow strength and grain size yield the greatest proportion of upslope-descending impacts (11). For smaller or larger grains, the interactions between hop trajectories and topography yield more downslope or upslope-ascending impacts, respectively.

4. Discussion

The results presented above demonstrate that incorporating bed topography into the saltation-abrasion model changes the results in three important ways. First, the magnitude of erosion is 10 to 1000 times greater, due to both the interception of saltation trajectories by topography and the increased kinetic energy transfer associated with high-angle impacts on the stoss side of bumps. Second, erosion increases with transport stage, whereas maximum erosion occurs at low to intermediate transport stage for planar topography. Third, erosion decreases with grain size, whereas maximal erosion occurs with intermediate-sized grains over the planar bed. Both the models with topography and the original planar saltation-abrasion model presented by *Sklar and Dietrich* [2004] are greatly simplified representations of complex processes. The goal of this discussion is to evaluate the implications of some of the prominent assumptions made within the modeling framework. At the end of the discussion, results from the modified saltation-abrasion model presented here are compared to experimental and field observations from the literature.

4.1. Effect of Topography on Flow

The magnitude of erosion for planar and nonplanar beds must be considered with regard to the effects of the bed topography on the flow. The topographic bump used for this analysis is small compared to the flow depth. A first-order calculation suggests that the bump would have to be about 10 times larger to cause a shift from subcritical to supercritical flow. However, increased form drag from the nonplanar bed will decrease τ^*, compared to the planar case. The nonplanar bed will also increase τ_c^*. Thus, transport stage will be lower for the nonplanar case at the same discharge.

The results presented above can be evaluated at "equal discharge" in several ways. First, the difference in erosion between the planar and the bump-normal case (Figure 7) can be viewed as a maximum estimate of the difference that would result from bed topography. Lower τ^*/τ_c^* is equivalent to shifting the bump-normal curve to the right in Figure 7. This reduces the difference in erosion rates. However, erosion is still much greater in the bump-normal case. For example, consider the case where discharge is such that $\tau^*/\tau_c^* = 10$ for the planar bed. Doubling τ_c^* to represent the effects of bed topography would yield a transport stage of $\tau^*/\tau_c^* = 5$. Bump-normal erosion is still about 100 times higher than for the planar case. Based on prior estimates of τ_c^* [e.g., *Chatanantavet et al.*, 2013, Table 2], doubling τ_c^* from 0.03 to 0.06 is a reasonable estimate for the difference in τ_c^* between the topographic bump used here and the "approximately planar" bed presented by *Sklar and Dietrich* [2004]. The only situation in which erosion would be greater in the planar case is when bed topography affects the flow so that τ^* is not above the transport threshold in the bump-normal case. This could happen at low flows or with relatively large sediment grains. Even if bed topography doubles τ_c^*, this condition would only exist over a very small range of the parameter space shown in Figures 7 and 8.

The effects of bed topography on erosion at equal discharge can also be considered by comparing the bump-normal and bump-vertical cases. Bed topography is the same in these two cases, so equal transport stage occurs at equal discharge. The difference in erosion between these cases is due to how erosion

is calculated. Only the vertical velocity (w_{si}) is used to calculate erosion in the bump-vertical case. In the bump-normal case, normal velocity (v_n) is calculated based on the impact angle, which depends on the saltation trajectory and the bed topography. This alone increases erosion by a factor of 5 to roughly 10, from low to high transport stage (Figure 7). This can be considered a minimum estimate of the change in erosion rate due to bed topography. The interception of saltation trajectories, which is identical in these two cases, would only make this difference greater.

A final issue associated with effects of the bed topography is related to flow separation. If the bump is large enough and the angle of the bump steep enough, flow separation can be induced. Flow separation will tend to increase the erosive effects of suspended load on the bed, as suspended sediment will be driven down into the lee side of the bump [e.g., *Hancock et al.*, 1998; *Whipple et al.*, 2000; *Wilson et al.*, 2013]. This process is not represented by any variants of the model presented here.

4.2. Effect of Topography on Impact Characteristics

In addition to lowering transport stage at a given discharge, the presence of topography will alter the near-bed velocity structure. A topographic bump will cause the flow to accelerate over the stoss side irregularity and decelerate over the lee side. This will affect the three types of impacts (Table 1) in different ways. Impacts on the downslope will be at angles steeper than those calculated since the flow decelerates on the lee side of the bump. The deceleration of the flow may also result in the grain impacting the bed with slower than calculated speeds. These two effects alter V_i in opposite directions.

Impacts on the upslope side of the bump during ascent will be accelerated by the flow over the bump. This will cause the impacts to occur at a smaller angle but with greater speed. Again, the effects of changes in ξ and S_i on V_i will oppose each other. In any case, this type of impact accounts for a very small percentage of the total erosion, so any changes will not greatly affect the results.

Finally, accelerating flow over the stoss side of the bump will tend to shallow out saltation trajectories that result in impacts that occur on the upslope during particle descent. This implies a reduction in ξ that would tend to reduce V_i. However, the faster flow may cause the impact to occur at a greater speed S_i, which would tend to increase V_i. Again, the two effects will act against each other. This type of impact accounts for a majority of erosion in the bump-normal model. Therefore, deviations from the calculated values would have the most significant effect on calculated erosion. The relative importance of changes in S_i and ξ will depend on the transport stage and grain size. Larger particles will be less affected by changes in the flow than smaller particles [*Anderson*, 1986].

In summary, for all impacts, the flow accelerating over the bump will cause deviations from the calculated values of impact angle and speed. These deviations, however, oppose each other, suggesting that the overall effect on V_i and therefore E will be small.

4.3. Particle Velocity Profiles

The horizontal velocity profile applied to the saltating grains (equations (12) and (15)) is defined in a piecewise fashion and therefore is an approximation of the physical system. As mentioned above, u along the ascent may be underestimated. An alternate approximation would be to assign $u_s = \overline{u_s}$ at all points along the trajectory, where $\overline{u_s}$ is defined by equation (14). This yields minimal changes in E for the base case, as the difference between $\overline{u_s}$ and u_{sf} is small and the effect of ascending particle impacts on the upslope is negligible (Table 1). Using $\overline{u_s}$ does not change the trends of E varying with τ^*/τ_c^* and D_s in Figures 7 and 8.

4.4. Use of Regression Statistics

In this study, regressions relating nondimensional excess shear stress to saltation characteristics from *Sklar and Dietrich* [2004] are used to simulate saltation trajectories and impacts. *Sklar and Dietrich* [2004] specifically note that their model does not simulate specific trajectories and instead use their regressions of data from several other saltation studies to capture average characteristics of saltating grains. Still, simulating trajectories from average characteristics will capture the average behavior of saltating grains. The approach presented here will effectively simulate the effect of saltating bed load over bed topography.

The regressions from *Sklar and Dietrich* [2004] rely on data from nine studies of saltation trajectory. Only one of these studies used grains larger than 10 mm [*Niño et al.*, 1994]. While *Sklar and Dietrich* [2004] use these regressions for larger grains ($D_s = 60$ mm), the data used to create these regressions do not extend to those grain sizes. Therefore, the reliability of the model decreases for grains larger than 10 mm. For this reason, the

base case in this study is $D_s = 5$ mm, which is in the middle of the grain sizes used in the studies used to create the regressions.

4.5. Distribution of Alluvial Cover

Here alluvial cover is treated as uniformly distributed across the streambed. By doing so, the cover effect can be accounted for using a single parameter (F_e). In reality, the alluvial cover will most likely exist as patches in topographic lows. This cover will reduce the number of impacts on both the upslope and the downslope at a ratio approximately equal to the ratio of their horizontal lengths. This means that the distribution of the alluvial cover will not greatly affect erosion rates, and treating F_e as a uniform random distribution of patches is a valid method of calculating E.

4.6. Agreement With Experimental Results and Field Observations

In addition to showing that bed topography increases erosion rates due to bed load, the results show that this erosion is focused on flow-facing slopes. Figure 5 (bottom) shows that nearly all of the erosion is on the stoss side of the bump. This finding is supported by results from flume experiments [e.g., *Johnson and Whipple*, 2010, Figure 9c] and observations in the field [e.g., *Whipple et al.*, 2000; *Johnson and Whipple*, 2007; *Goode and Wohl*, 2010; *Wilson et al.*, 2013].

Wilson et al. [2013] investigated the processes that form and erode bedforms shaped much like the bump used in this study. Upstream-facing convex surfaces are widespread and are formed with a crest line perpendicular to flow [*Richardson and Carling*, 2005]. Based on observations in the field and in flow experiments, *Wilson et al.* [2013] argued that these bedforms are formed and shaped by bedload abrasion. In the absence of flow separation, erosion is concentrated on the upstream face, where most impacts occur. The model presented here matches these observations. However, in the case of flow separation, erosion is dominated by suspended load abrasion and is concentrated on the lee side of bumps [e.g., *Hancock et al.*, 1998; *Whipple et al.*, 2000; *Wilson et al.*, 2013].

5. Conclusions

Simple bed topography can increase erosion rates due to abrasion by bed load by orders of magnitude, even if the topography is small and low angle. This enhanced erosion is focused on flow-facing slopes, as seen in the field [e.g., *Whipple et al.*, 2000; *Wilson et al.*, 2013] and in flume experiments [e.g., *Johnson and Whipple*, 2010]. Compared to a planar bed, erosion is enhanced by two different processes. First, bed topography intercepts saltation trajectories, increasing the impact rate. This is most important at high transport stage. Second, horizontal grain velocity, which is an order of magnitude greater than settling velocity, dominates impact kinetic energy when bed topography is considered. With simple bed topography, erosion is greatest at high transport stage and with small grains. This is in contrast to the findings of *Sklar and Dietrich* [2004], who predicted maximum erosion at low to intermediate transport stage and with medium-sized grains. This finding is independent of the angle of the topography. Therefore, it is important to consider the effects of bed topography when modeling erosion in bedrock streams.

Notation

A_{tot}	total area traversed
A_u	area traversed over upslope
A_d	area traversed over downslope
D_s	sediment grain diameter
E	erosion rate
E_u	erosion rate on upslope
E_d	erosion rate on downslope
E_f	erosion rate over flat topography
F_e	exposed fraction of the bed
Fr	Froude number
H_s	saltation hop height
H_w	flow depth
I_r	impact rate per unit area
I_{ru}	impact rate per area on upslope

I_{rd}	impact rate per area on downslope
$\overline{L_s}$	average saltation hop length
L_s	hop length of specific hop
L_{sd}	length of specific hop descent
$\overline{L_{sd}}$	average length of saltation descent
L_{su}	length of saltation hop ascent
R_b	nondimensional buoyant density
S_i	impact speed
V_i	volume eroded per impact
Y	Young's modulus of the bed
g	gravitational acceleration
h_c	critical flow depth
i_u	upslope impact rate (per particle)
i_d	downslope impact rate (per particle)
k_v	dimensionless coefficient = 10^6
l	total horizontal length of topography
l_{up}	horizontal length of upslope
m	mass flux per width per particle
n	number of impacts
n_u	number of impacts on upslope
n_d	number of impacts on downslope
n_m	Manning's roughness of the channel
q_s	sediment mass flux per width
q_t	transport capacity per width
t_{tot}	total time of simulation
t_u	time spent above upslope
t_d	time spent above downslope
u	downstream flow velocity
u_{sf}	horizontal sediment velocity at takeoff elevation
u_{si}	horizontal sediment velocity at impact
$\overline{u_s}$	average horizontal sediment velocity
u_{su}	horizontal sediment velocity along ascent
u_*	friction velocity
v_n	normal sediment impact velocity
w_{si}	vertical sediment velocity at impact
w_{sd}	mean sediment descent velocity
w_{sf}	vertical sediment velocity at takeoff elevation
$\overline{w_{sf}}$	mean w_{sf}
w'	deviatoric vertical sediment velocity
x	horizontal position of sediment grain
z	vertical position of sediment grain
θ	angle of flow-facing slope
ξ	impact angle
ρ_s	density of sediment grains
ρ_w	density of water
σ_T	tensile yield stress of the bed
τ_b	basal shear stress
τ^*	dimensionless basal shear stress
τ_c^*	τ^* at threshold of particle motion
τ^*/τ_c^*	transport stage
$\tau^*/\tau_c^* - 1$	nondimensional excess shear stress
ψ	saltation takeoff angle

Acknowledgments
This research is supported by a grant from the National Science Foundation Geomorphology and Land Use Dynamics Program (EAR 0922235). The manuscript was greatly improved by insightful comments from Robert Anderson and Greg Tucker and from reviews by Dimitri Lague, Phairot Chatanantavet, and an anonymous reviewer.

References

Abbott, J. E., and J. R. D. Francis (1977), Saltation and suspension trajectories of solid grains in a water stream, *Philos. Trans. R. Soc. London, Ser. A*, *284*, 225–254, doi:10.1098/rsta.1977.0009.

Allen, J. (1971), Transverse erosional marks of mud and rock: Their physical basis and geological significance, *Sediment. Geol.*, *5*, 167–385, doi:10.1016/0037-0738(71)90001-7.

Anderson, R. S. (1986), Erosion profiles due to particles entrained by wind: Application of an eolian sediment-transport model, *Geol. Soc. Am. Bull.*, *97*, 1270, doi:10.1130/0016-7606(1986)97<1270:EPDTPE>2.0.CO;2.

Anderson, R. S. (1994), Evolution of the Santa Cruz Mountains, California through tectonic growth and geomorphic decay, *J. Geophys. Res.*, *99*, 20,161–20,179, doi:10.1029/94JB00713.

Anderson, R. S., and P. K. Haff (1988), Simulation of eolian saltation, *Science*, *241*(4867), 820–823, doi:10.1126/science.241.4867.820.

Barnes, H. L. (1956), Cavitation as a geological agent, *Am. J. Sci.*, *254*, 493–505, doi:10.2475/ajs.254.8.493.

Chatanantavet, P., and G. Parker (2009), Physically based modeling of bedrock incision by abrasion, plucking, and macroabrasion, *J. Geophys. Res.*, *114*, F04018, doi:10.1029/2008JF001044.

Chatanantavet, P., K. X. Whipple, M. A. Adams, and M. P. Lamb (2013), Experimental study on coarse grain saltation dynamics in bedrock channels, *J. Geophys. Res. Earth Surf.*, *118*, 1161–1176, doi:10.1002/jgrf.20053.

D'Errico, J. (2009), SLM—Shape language modeling, *MATLAB Central File Exchange*, (updated 2012). [Available at http://www.mathworks.com/matlabcentral/fileexchange/24,443--slm--shape--language--modeling.]

Einstein, H. A. (1950), The bed-load function for sediment transportation in open channel flows, *Technical Bulletin 1026*, U. S. Dept. of Agriculture, Soil Conversation Service.

Engel, P. A. (1976), *Impact Wear of Materials*, 339 pp., Elsevier Scientific Pub. Co., New York.

Fernandez-Luque, R., and R. van Beek (1976), Erosion and transport of bed-load sediment, *J. Hydraul. Res.*, *14*, 127–144.

Finnie, I. (1960), Erosion of surfaces by solid particles, *Wear*, *3*(2), 87–103, doi:10.1016/0043-1648(60)90055-7.

Goode, J. R., and E. Wohl (2010), Substrate controls on the longitudinal profile of bedrock channels: Implications for reach-scale roughness, *J. Geophys. Res.*, *115*, F03018, doi:10.1029/2008JF001188.

Hancock, G. S., and R. S. Anderson (2002), Numerical modeling of fluvial strath-terrace formation in response to oscillating climate, *Geol. Soc. Am. Bull.*, *114*(9), 1131–1142, doi:10.1130/0016-7606(2002)114<1131:NMOFST>2.0.CO;2.

Hancock, G. S., R. S. Anderson, and K. X. Whipple (1998), Beyond power: Bedrock river incision process and form, in *Rivers Over Rock: Fluvial Processes in Bedrock Channels, Geophys. Monogr. Ser.*, vol. 107, edited by J. Tinkler and E. Wohl, pp. 35–60, AGU, Washington, D. C., doi:10.1029/GM107p0035.

Hancock, G. S., E. E. Small, and C. Wobus (2011), Modeling the effects of weathering on bedrock-floored channel geometry, *J. Geophys. Res.*, *116*, F03018, doi:10.1029/2010JF001908.

Howard, A. D., W. E. Dietrich, and M. A. Seidl (1994), Modeling fluvial erosion on regional to continental scales, *J. Geophys. Res.*, *99*, 13,971–13,986, doi:10.1029/94JB00744.

Hu, C., and Y. Hui (1996a), Bed-load transport. I: Mechanical characteristics, *J. Hydraul. Eng.*, *122*(5), 245–254, doi:10.1061/(ASCE)0733-9429(1996)122:5(245).

Hu, C., and Y. Hui (1996b), Bed-load transport. II: Stochastic characteristics, *J. Hydraul. Eng.*, *122*(5), 255–261, doi:10.1061/(ASCE)0733-9429(1996)122:5(255).

Johnson, J. P., and K. X. Whipple (2007), Feedbacks between erosion and sediment transport in experimental bedrock channels, *Earth Surf. Processes Landforms*, *32*(7), 1048–1062, doi:10.1002/esp.1471.

Johnson, J. P. L., and K. X. Whipple (2010), Evaluating the controls of shear stress, sediment supply, alluvial cover, and channel morphology on experimental bedrock incision rate, *J. Geophys. Res.*, *115*, F02018, doi:10.1029/2009JF001335.

Lamb, M. P., W. E. Dietrich, and L. S. Sklar (2008), A model for fluvial bedrock incision by impacting suspended and bed load sediment, *J. Geophys. Res.*, *113*, F03025, doi:10.1029/2007JF000915.

Lee, H.-Y., and I.-S. Hsu (1994), Investigation of saltating particle motions, *J. Hydraul. Eng.*, *120*(7), 831–845, doi:10.1061/(ASCE)0733-9429(1994)120:7(831).

Montgomery, D. R., and J. M. Buffington (1997), Channel-reach morphology in mountain drainage basins, *Geol. Soc. Am. Bull.*, *109*(5), 596–611, doi:10.1130/0016-7606(1997)109<0596:CRMIMD>2.3.CO;2.

Nasrollahi, A., S. A. A. Salehi Neyshabouri, G. Ahmadi, and M. M. Namin (2008), Numerical simulation of particle saltation process, *Part. Sci. Technol.*, *26*(6), 529–550, doi:10.1080/02726350802498723.

Nezu, I., and H. Nakagawa (1993), *Turbulence in Open-Channel Flows*, 281 pp., Balkema, Rotterdam, The Netherlands.

Niño, Y., M. Garcia, and L. Ayala (1994), Gravel saltation: 1. Experiments, *Water Resour. Res.*, *30*(6), 1907–1914, doi:10.1029/94WR00533.

Richardson, K., and P. Carling (2005), *Typology of Sculpted Forms in Open Bedrock Channels,* Special Paper 392, 108 pp., Geol. Soc. of Am., Boulder, Colo.

Rubinow, S. I., and J. B. Keller (1961), The transverse force on a spinning sphere moving in a viscous fluid, *J. Fluid Mech.*, *11*, 447–459, doi:10.1017/S0022112061000640.

Sekine, M., and H. Kikkawa (1992), Mechanics of saltating grains. II, *J. Hydraul. Eng.*, *118*(4), 536–558, doi:10.1061/(ASCE)0733-9429(1992)118:4(536).

Sklar, L. S. (2003), The influence of grain size, sediment supply, and rock strength on rates of river incision into bedrock, Univ. of California, Berkeley.

Sklar, L. S., and W. E. Dietrich (2001), Sediment and rock strength controls on river incision into bedrock, *Geology*, *29*, 1087, doi:10.1130/0091-7613(2001)029<1087:SARSCO>2.0.CO;2.

Sklar, L. S., and W. E. Dietrich (2004), A mechanistic model for river incision into bedrock by saltating bed load, *Water Resour. Res.*, *40*, W06301, doi:10.1029/2003WR002496.

Stock, J. D., and D. R. Montgomery (1999), Geologic constraints on bedrock river incision using the stream power law, *J. Geophys. Res.*, *104*, 4983–4993, doi:10.1029/98JB02139.

Tucker, G. E., and R. L. Slingerland (1994), Erosional dynamics, flexural isostasy, and long-lived escarpments: A numerical modeling study, *J. Geophys. Res.*, *99*, 12,229–12,243, doi:10.1029/94JB00320.

Turowski, J. M., D. Lague, and N. Hovius (2007), Cover effect in bedrock abrasion: A new derivation and its implications for the modeling of bedrock channel morphology, *J. Geophys. Res.*, *112*, F04006, doi:10.1029/2006JF000697.

Turowski, J. M., N. Hovius, H. Meng-Long, D. Lague, and C. Men-Chiang (2008), Distribution of erosion across bedrock channels, *Earth Surf. Processes Landforms*, *33*, 353–363, doi:10.1002/esp.1559.

Whipple, K. X. (2004), Bedrock rivers and the geomorphology of active orogens, *Annu. Rev. Earth Planet. Sci.*, *32*, 151–185, doi:10.1146/annurev.earth.32.101802.120356.

Whipple, K. X., and G. E. Tucker (1999), Dynamics of the stream-power river incision model: Implications for height limits of mountain ranges, landscape response timescales, and research needs, *J. Geophys. Res.*, *104*, 17,661–17,674, doi:10.1029/1999JB900120.

Whipple, K. X., and G. E. Tucker (2002), Implications of sediment-flux-dependent river incision models for landscape evolution, *J. Geophys. Res.*, *107*(B2), 2039, doi:10.1029/2000JB000044.

Whipple, K. X., G. S. Hancock, and R. S. Anderson (2000), River incision into bedrock: Mechanics and relative efficacy of plucking, abrasion, and cavitation, *Geol. Soc. Am. Bull.*, *112*(3), 490–503, doi:10.1130/0016-7606(2000)112<490:RIIBMA>2.0.CO;2.

Wiberg, P. L., and J. D. Smith (1985), A theoretical model for saltating grains in water, *J. Geophys. Res.*, *90*, 7341–7354, doi:10.1029/JC090iC04p07341.

Wilson, A., N. Hovius, and J. M. Turowski (2013), Upstream-facing convex surfaces: Bedrock bedforms produced by fluvial bedload abrasion, *Geomorphology*, *180*, 187–204, doi:10.1016/j.geomorph.2012.10.010.

Wobus, C. W., G. E. Tucker, and R. S. Anderson (2006), Self-formed bedrock channels, *Geophys. Res. Lett.*, *33*(18), L18408, doi:10.1029/2006GL027182.

Wohl, E. E. (1993), Bedrock channel incision along Piccaninny Creek, Australia, *J. Geol.*, *101*, 749–761, doi:10.1086/648272.

Wohl, E. E., and H. Ikeda (1997), Experimental simulation of channel incision into a cohesive substrate at varying gradients, *Geology*, *25*, 295, doi:10.1130/0091-7613(1997)025<0295:ESOCII>2.3.CO;2.

Wohl, E. E., and H. Ikeda (1998), Patterns of bedrock channel erosion on the Boso Peninsula, Japan, *J. Geol.*, *106*, 331–346, doi:10.1086/516026.

Wohl, E. E., and D. M. Merritt (2001), Bedrock channel morphology, *Geol. Soc. Am. Bull.*, *113*(9), 1205–1212, doi:10.1130/0016-7606(2001)113<1205:BCM>2.0.CO;2.